FACTA UNIVERSITATIS
Series: **Mechanics, Automatic Control and Robotics** Vol.3, N° 13, 2003, pp. 533 - 552

FAILURE METHODOLOGY OF MODE-II LOADED CRACKS

UDC 539.219.2 620.1

Jörg F. Kalthoff

Experimental Mechanics, Ruhr-University Bochum, 44780 Bochum, Germany
e-mail: Joerg.F.Kalthoff@ruhr-uni-bochum.de

Abstract. *Various aspects of the failure behaviour initiated from mode-II loaded cracks are discussed: validity criteria and minimum size specimen requirements for measuring the fracture toughness K_{IIc}; energy balance of the process of initiation of kinked cracks including compressive notch tip stress concentrations; failure mode transition from tensile cracks to adiabatic shear bands at high loading rates; loading rate dependence of the dynamic fracture toughness K_{IId} in the regime of failure mode transition. Findings of studies on these subjects are presented and implications of the results for practical applications are discussed. The failure behaviour of mode-II loaded cracks is found very different and far more complicated than of mode-I loaded cracks, generalizations from mode-I to mode-II can therefore be severely misleading.*

INTRODUCTION

Fracture mechanics investigations mostly deal with tensile mode-I situations of loading. One practical implication of this situation is that standards for measuring fracture properties of materials subjected to tensile mode-I conditions of loading have been developed and are available, but any standards for measuring mode-II or mixed mode-I/mode-II failure properties do not exist. Many applications in practice, however, deal with mode-II or mixed mode loading situations. These cases are often treated according to what is known and specified for the mode-I loading case. This paper is aimed to show that the failure behaviour of mode-II and mixed mode loaded cracks is principally different from the one of mode-I loaded cracks, that erroneous results can be obtained when failure properties for mode-II or mixed mode loading situations are measured following the principles developed for mode-I loading, and, that the failure behaviour for mode-II loading situations at increasing levels of loading rate shows phenomena that do not become activated and that do not exist for mode-I loading situations. Given are results and conclusions that have been presented at the Yokobori Conference on Complexity and Frontiers in Strength and Fracture in Sendai, Japan in 2001 [1].

Received October 20, 2002

VALIDITY CRITERIA FOR MEASURING THE MODE-II FRACTURE TOUGHNESS K_{IIc}

For tensile mode-I conditions of loading validity criteria have been established that have to be met in order to allow for an application of the concept of linear-elastic or small scale yielding fracture mechanics and for measuring the fracture toughness of the material. These criteria, formulated for fracture toughness tests, are given in the form of minimum specimen size requirements in the stand-ard ASTM E 399 [2]. When the characteristic measurement of the specimen in out-of-plain direc-tion, i.e. the thickness of the specimen, is larger than $2.5(K_{Ic}/\sigma_{YS})^2$, where K_{Ic} = plane strain fracture toughness, σ_{YS} = yield strength, a dominating state of plane strain applies at the crack tip. Further-more, when the characteristic measurements of the specimen in in-plane directions, i.e. the height of the specimen, the length of the crack, and the length of the ligament, are larger than this same quan-tity mentioned above, the conditions of linear-elastic or small scale yielding fracture mechanics are fulfilled, i.e. a stress intensity factor description based on the K-concept can be used to characterize the crack tip stress field. Under these conditions the concept of LEFM allows failure predictions with the plane strain fracture toughness K_{Ic} as material property. The criteria are based on the size of the crack tip plastic zones, specifically the dependency of the size of the zone across the thick-ness of the specimen and the size in relation to the in-plane dimensions of the specimen. Equivalent minimum size requirements and validity criteria for in-plane shear (mode-II) conditions of loading do not exist. Efforts were undertaken by Hiese and Kalthoff to develop such criteria [3,4].

Following in principle the argumentation that led to the well known minimum size specimen requirements in the mode-I case, the plastic zones at the tip of mode-II loaded cracks were considered and on this basis validity criteria were developed for mode-II test. For the two cases of plane strain and plane stress, Fig. 1 shows the mode-II crack tip plastic zones in comparison to equivalent (i.e. $K_{II} = K_I$) mode-I crack tip plastic zones. Two characteristic differences are recognized: First, for mode-II loading the overall size of the plastic zones is considerably larger, but, secondly, the differences of the plastic zones for the stress states of plane strain and plane stress are considerably smaller than for the equivalent case of mode-I loading.

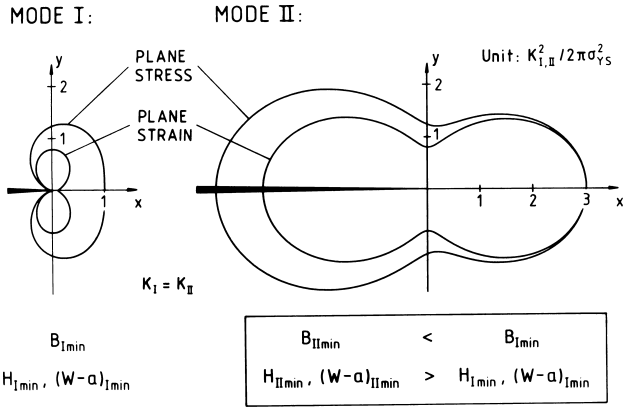

Fig. 1. Crack tip plastic zones for mode-I and mode-II conditions of loading.

Because of these differences in the plastic zones it is concluded that the usual requirements for a K_{Ic}-test cannot be adopted for a K_{IIc}-test. The relatively small differences in size of the mode-II zones for the conditions of plane strain and plane stress will obviously allow smaller minimum specimen thicknesses $B_{II\,min}$ for a mode-II test than for a mode-I test. Because of the larger overall size of the plastic zones, however, the in-plane specimen dimensions, i.e. the height $H_{II\,min}$ and the ligament length $(W\text{-}a)_{II\,min}$ of the specimen should be larger than for a mode-I test. If one assumes that the fracture behaviour is controlled by the size of the plastic zone, where the size shall be given by the averaged radius of the plastic zone for the moment, one would speculate that the thickness $B_{II\,min}$ should be about three times smaller, the height $H_{II\,min}$ and the ligament length $(W\text{-}a)_{II\,min}$, however, should be about four times larger than for a mode-I test. With the quantitative estimate of the mode-I size requirements transferred in an analogous manner to mode-II, the specimen size requirements for valid K_{IIc}-tests would result in

$$B_{II} > 0.8\left(\frac{K_{IIc}}{\sigma_{YS}}\right)^2 \tag{1}$$

$$H_{II} > 10\left(\frac{K_{IIc}}{\sigma_{YS}}\right)^2 \quad \text{and} \quad (W-a) > 10\left(\frac{K_{IIc}}{\sigma_{YS}}\right)^2 . \tag{2}$$

In order to verify these postulated hypothesis, mode-I and mode-II fracture toughnesses were measured with specimens of different sizes made of the aluminum alloy Al 7075 and the tool steel 90 MnCrV 8. The relevant material properties of the aluminum alloy Al 7075 in the condition as used for the investigations are: $K_{Ic} = 27$ MN/m$^{3/2}$, $\sigma_{YS} = 488$ MPa (TL-orientation), and $K_{Ic} = 30$ MN/m$^{3/2}$, $\sigma_{YS} = 533$ MPa (LT-orientation). The steel 90 MnCrV 8 was used in different conditions that were achieved by different heat treatments: For the same hardening temperature of 950 °C the tempering temperature was varied from 630 °C to 570 °C to result in material properties varying from $K_{Ic} = 70$ MN/m$^{3/2}$, $\sigma_{YS} = 1000$ MPa to $K_{Ic} = 56$ MN/m$^{3/2}$, $\sigma_{YS} = 1130$ MPa.

The fracture toughness tests were performed with loading fixtures of the modified Arcan/Richard-type [5, 6], shown schematically in Fig. 2. The test specimens were equipped with machined Chevron-type prenotches, which were subsequently fatigue loaded under mode-I conditions according to ASTM E 399 in order to achieve standard initial starter cracks. The same mode-I fatigue loading procedure was applied to specimens used for both the mode-II and the mode-I fracture tests. The test conditions have been chosen to result to a large extent in invalid results in order to establish a data base for investigating the range where the validity of the data gets lost. In the invalid regimes, but also in the regime of valid tests, the mode-II and the mode-I fracture toughnesses were determined using the 5 % secant evaluation procedure as described in ASTM E 399. The measured mode-II and mode-I fracture toughness values as determined after the test, without having been approved by validity conditions yet, are denoted K_{IIQ} and K_{IQ} respectively.

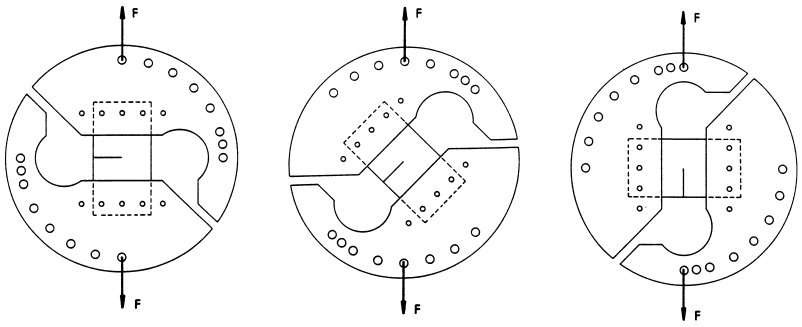

Fig. 2. Mixed mode loading fixture after Arcan, Richard.

The measured mode-II and mode-I fracture toughnesses are summarized in Figs. 3 and 4. The data are shown as functions of the characteristic out-of-plane dimension, i.e. the thickness B of the specimen, and as functions of the characteristic in-plane dimensions, i.e. the height H and the ligament length (W-a) of the specimen. In order to allow for a joint presentation of all the data determined for the different materials and conditions, the data are normalized with respect to their respective fracture toughness values.

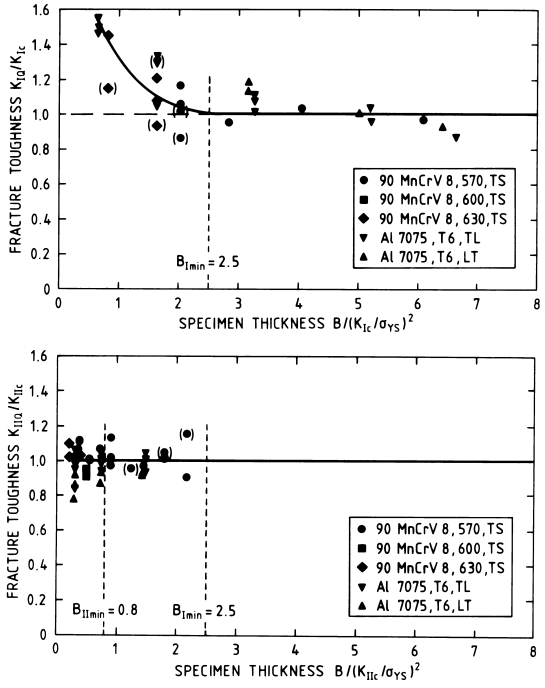

Fig. 3. Dependence of the mode-II fracture toughness from specimen thickness in comparison to the mode-I behaviour. Normalized plots for data measured with Al 7075 and steel 90 MnCrV 8.

As regards the specimen thickness requirement for determining valid fracture toughnesses, the results indicate the usual behaviour when the mode-I fracture toughness K_{Ic} is considered: A practically constant value is obtained for thicknesses above $2.5(K_{Ic}/\sigma_{YS})^2$; for thicknesses smaller than this value the measured fracture toughness values show an increasing tendency. This behaviour is in full accordance with what is expected according to the standard ASTM E 399. For the mode-II fracture toughness K_{IIc}, however, practically constant toughness values are found for thicknesses below the critical thickness of mode-I tests, i.e. constant mode-II fracture toughnesses are found in the regime of thicknesses where the mode-I fracture toughnesses show a strongly increasing tendency. Practically constant mode-II fracture toughnesses are obtained down to thicknesses of about $0.5(K_{IIc}/\sigma_{YS})^2$, i.e. for thicknesses even somewhat lower than predicted by the postulated hypothesis.

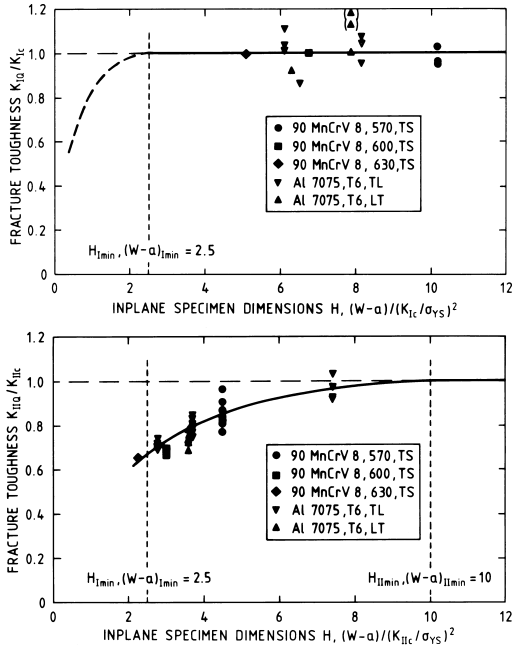

Fig. 4. Dependence of the mode-II fracture toughness from in-plane specimen dimensions in comparison to the mode-I behaviour. Normalized plots for data measured with Al 7075 and steel 90 MnCrV 8.

As regards the minimum in-plane dimensions of the specimen, i.e. H and (W-a), for determining valid fracture toughnesses, the data indicate the following behaviour. For the mode-I fracture toughness K_{Ic} practically constant values were measured with specimens of in-plane dimensions H and (W-a) well above the value $2.5(K_{Ic}/\sigma_{YS})^2$, as it is expected according to ASTM E 399. For the mode-II fracture toughness K_{IIc}, however, non-constant values are measured with specimens of dimensions H and (W-a) above the critical in-plane dimensions for mode-I tests, i.e. non-constant mode-II fracture toughnesses are found in the regime of in-plane dimensions of the specimen where the mode-I fracture toughness does show constant values already. The data indicate that constant mode-II fracture toughnesses are approached at larger dimensions of about $10(K_{IIc}/\sigma_{YS})^2$ only.

Thus, the experimental findings as regards the minimum thickness as well as the minimum in-plane dimensions of specimens fully verify the postulated hypothesis (1) and (2) for performing valid mode-II fracture toughness tests.

The investigations have shown that mode-II crack tip plastic zones are considerably larger than equivalent mode-I crack tip plastic zones, and, therefore, that the in-plane dimensions of mode-II test pieces have to be considerably larger than for mode-I cases to fulfill the conditions of linear-elastic or small scale yielding fracture mechanics. It is speculated that many so called shear fracture toughness data reported in the literature represent invalid data, since they were not determined according to these novel criteria, but in very many cases were measured with specimens following in principle the requirements for a mode-I test. The fact, that such literature data are not valid in the above mentioned sense may also be one of the reasons for such controversies that in some cases shear fracture toughnesses "K_{IIc}" were reported lower but in other cases higher than the tensile fracture toughness K_{Ic}.

INSTABILITY PROCESS OF MODE-II LOADED CRACKS

The process of instability of a mode-I loaded crack is rather simple in nature: The crack extends straight in its original direction, and, as a consequence, the mode-I crack tip stress field before instability stays a mode-I stress field after instability. The situation is more complex for a mode-II loaded crack: the direction of propagation of the initiated crack after instability is different from the direction of the initial mother crack; the crack propagates at an angle of about 70° with respect to the ligament and, in conjunction with it, the crack tip stress field changes from mode-II before instability to mode-I after instability.

The instability process of mode-II loaded cracks has been investigated by Podleschny and Kalthoff [7, 8]. In these studies not only the phase directly before instability is considered - which is the phase that is usually considered in investigations of the instability event - but also the phase after instability is considered, i.e. the phase of propagation of the initiated kinked crack.

In the investigations the instability process of mode-II loaded cracks has been monitored by means of the shadow optical method of caustics in combination with high speed photography. Figure 5 shows shadowgraphs of the situation a short time after instability. A review on the principles of the shadow optical method of caustics for measuring stress concentrations is given in [9]. In addition to the mode-I stress intensification field which builds up at the tip of the kinked crack that is initiated from the mode-II loaded mother crack - this stress intensification field is trivially expected - another stress concentration field is found which builds up at the notch that is formed between the initiated kinked crack and the original mother crack (see dark shadow spot in Fig. 5, lower part). Figure 6 shows the result of equivalent photo-elastic investigations performed with a model experiment. The fringe patterns Fig. 6b and c which simulate the loading situation after instability in a quasi-static saw cut approximation show a tensile (mode-I) loading at the tip of the simulated kinked crack and an additional stress concentration at the formed notch, i.e. the fringe patterns give evidence of the same behaviour as derived from the shadow optical picture. The stress concentration field that additionally builds up at the notch tip is a compressive field, as is demonstrated by the character of the shadow pattern (see [9]). Thus, the shear mode-II stress intensification field around the tip of a starter crack before

instability is not only transferred into a tensile mode-I stress intensification field at the tip of the initiated kinked crack after instability, but, parts of the original shear mode-II field are also transferred into a compressive stress concentration field at the notch that is formed.

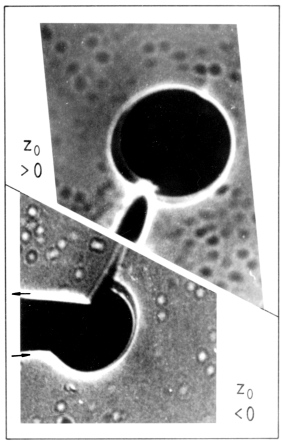

Fig. 5. Shadow optical simulation of the post instability loading situation of a shear mode-II loaded mother crack, indicating a tensile mode-I loading at the tip of the initiated kinked crack (real shadowgraph, $z_0 > 0$, upper part) and an additional compressive stress concentration at the notch formed between the initiated kinked crack and the original mother crack (virtual shadowgraph, $z_0 < 0$, lower part). Shadowgraphs recorded in transmission with an epoxy resin specimen.

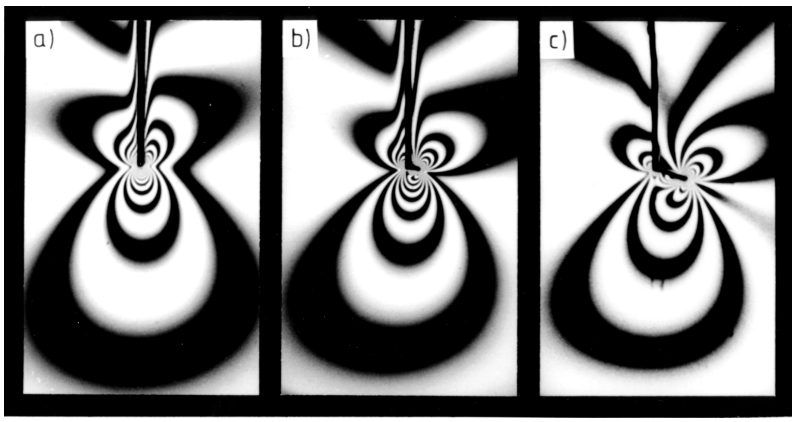

Fig. 6. Photoelastic visualization of changes of the loading situation of a shear mode-II loaded mother crack from (a) before to (b), (c) after instability. Quasi-static investigation with saw cut model.

Figure 7 illustrates this behaviour (lower graphs) and shows the situation in comparison to the simpler case of mode-I loading (upper graphs). Completely analogous behaviour results for cracks under mixed mode-II/mode-I conditions of loading. Of course, the larger the mode-I contribution, the shallower the notch; and, trivially, for non-existing mode-II contributions, the notch does not exist and the crack shows the usual straight propagation behaviour. With respect to these post instability processes, which are very different in nature for mode-I and mode-II loaded cracks, it is concluded that the mode-I instability process represents a much simpler event than the mode-II instability process. Thus, any attempts to transfer fracture mechanics criteria and validity conditions from mode-I to mode-II loading in one way or another must principally fail, since completely new and different processes which do not exist for mode-I loading come additionally into play for mode-II loading.

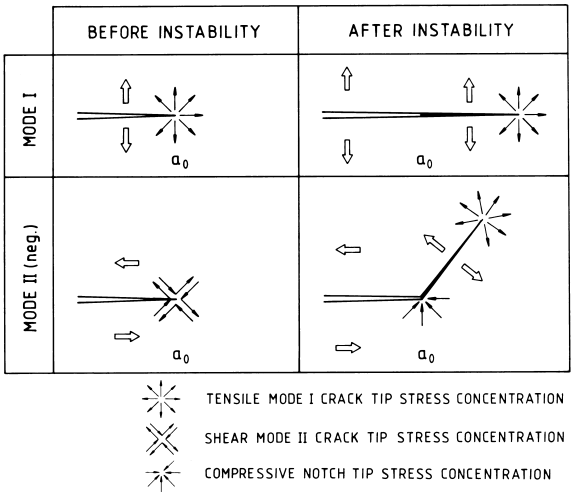

Fig. 7. Differences in the instability process of tensile mode-I and shear mode-II loaded cracks, schematically.

The elastic energies stored in the three types of stress concentration fields that control the instability process of mode-II loaded cracks, i.e. a mode-II and a mode-I crack tip field, and the compressive notch tip field, have been quantified. In addition to the pure mode-II loading situation, the general case of mixed mode-II/mode-I loading, and, consequently, compressive notch tip fields of various notch angles, are considered. In order to allow for an easy comparison of data, all energy quantities are given in normalized form relative to the energy stored at the tip of a tensile mode-I loaded crack. The different singularities of the crack tip stress field ($r^{-0.5}$) and of the notch tip field ($r^{-0.415}$ for a 70° notch) have been taken care of in the calculations; but, whereas exact expressions were de-rived for the crack tip energies only approximate relationships are given for the notch tip energy [7].

For clarity of presentation, in addition to the subscripts '$_I$' and '$_{II}$' for characterization of the stress intensity factors for conditions of mode-I and mode-II loading respectively, the subscripts '$_{MM}$' are added when mixed mode loading conditions apply and both stress

intensity factors K_I and K_{II} exist simultaneously, whereas the subscript '$_{PM}$' is added when pure conditions of either mode-I or mode-II loading apply. Using this nomenclature the following expressions are derived for the crack tip energy U_C and the notch tip energy U_N (see [8])

$$\frac{U_{C,MM}}{U_{C,PM}} = \left(K_{MMI}^2 + \frac{2\kappa+3}{2\kappa-1} K_{MMI}^2 \right) \frac{1}{K_{PMI}^2} \quad \text{and} \quad \frac{U_{N,MM}}{U_{C,MM}} = \frac{1}{4} \left(\frac{K_{MMII}}{K_{MMI} + K_{MMII}} \right)^{5/2} \tag{3}$$

with $\kappa = (3-\nu)/(1+\nu)$ for plane stress,
$\kappa = 3-4\nu$ for plane strain,

where

U_C = elastic energy stored around a crack
U_N = elastic energy stored around a notch that is formed by a crack initiation under mixedmode loading conditions
K = stress intensity factor
$_{PMI}$, $_{PMII}$ = subscripts characterizing a pure mode-I or a pure mode-II loading condition
$_{MM}$ = index characterizing mixed mode conditions of loading
$_{MMI}$, $_{MMII}$ = indices characterizing the mode-I or the mode-II portion of a mixed mode loading condition.

Figure 8 shows the dependence of the crack tip energy U_C and of the notch tip energy U_N as function of the ratio of mode mixity assuming equivalent loading conditions, i.e. $(K_{MMI}^2 + K_{MMII}^2)^{1/2} = K_{PMI} = K_{PMII}$. Data are given for the states of plane stress and plane strain and different values of Poisson's ratio.

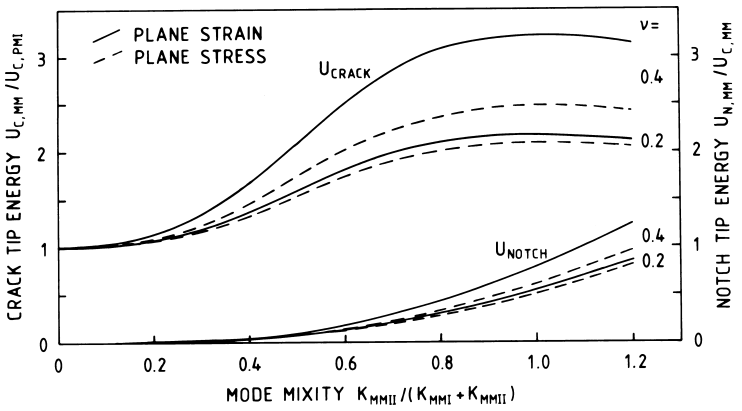

Fig. 8. Elastic energies of crack tip and notch tip stress fields for different mode mixities.

It is recognized: First, for a mode-II loaded crack the stored elastic energy is roughly a factor of three larger than the elastic energy stored at a mode-I loaded crack, provided that an equivalency of the form $K_{PMI} = K_{PMII}$ is given. Secondly, for a mode-II loaded crack the elastic energy stored at the notch that is additionally formed between the initiated kinked crack and the original mother crack is roughly one quarter of the elastic en-

ergy stored at the original mode-II loaded mother crack. Consequently, for the first step of crack propagation after instability only the difference of these two energy quantities represents the energy that is available for building up the stress concentration at the tip of the initiated kinked crack. Only this difference energy is available for crack extension, i.e. represents the crack driving energy. For mixed mode conditions of loading shallower notches result and the energy quantities are accordingly lower; for a crack under pure mode-I loading the notch tip energy is trivially zero. On the basis of this difference energy approach an expression for the strain energy release rate for kinked crack propagation has been developed, given in [7, 8].

The validity of the derived expressions was verified by experimental investigations: For cracks that were initiated from starter cracks that were loaded under pure mode-II and pure mode-I conditions of loading the stress intensity factors and the velocities of the propagating cracks were determined at short times after instability. The data were obtained by means of the shadow optical method of caustics in combination with high speed photography. Experiments were performed with specimens made from the model material Araldite B loaded quasi-statically in the modified Arcan/Richard mixed mode loading fixture. Typical results obtained for a crack initiated under pure mode-I and under almost pure mode-II conditions of loading are shown in Fig. 9. In the so-called "mode-II" loading experiment on purpose, a small amount of mode-I loading was superimposed to the dominating mode-II loading in order to avoid disturbances in the fracture behaviour that might be caused by friction effects between the fracture surfaces. But, the magnitude of the superimposed mode-I loading is very small (see data point for t = 0 in Fig. 9) and, thus, can be neglected in the following consideration. Figure 9 shows the dynamic stress intensity factors K_i and the velocity v of the propagating cracks after initiation as functions of time t after instability. Due to special treatments of the crack tip regions, the two cracks - although subjected to different loading modes - were initiated under almost the same value of the stress intensity factors: In the mode-I experiment the crack was initiated at $K_{PMI,c}$ ($\equiv K_{Ic}$ in usual nomenclature) = 0.67 $MN/m^{3/2}$; in the "mode-II" experiment the crack was initiated at a critical stress intensity factor of $K_{MMII,c} \approx K_{PMII,c}$ ($\equiv K_{IIc}$ in usual nomenclature) = 0.57 $MN/m^{3/2}$.

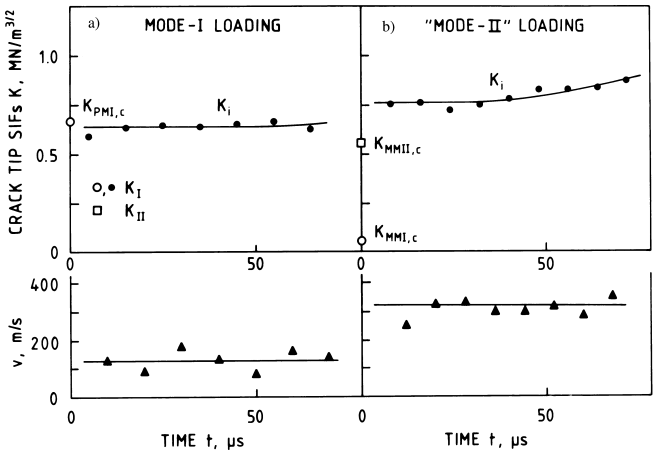

Fig. 9. Post instability failure behaviour of cracks initiated under mode-I and mode-II conditions of loading.

The following behaviour is recognized: Although the critical stress intensity factors at instability for the mode-II and for the mode-I experiment are (very roughly) similar, or, more precisely, although the critical stress intensity factor in the mode-II experiment was even somewhat lower than the critical stress intensity factor in the mode-I experiment, the stress intensity factors K_i of the crack initiated under mode-II conditions of loading are considerably higher than those measured for the crack initiated under mode-I conditions of loading. The higher stress intensity factors are supported by the accompanying higher crack propagation velocities. These experimental findings are in qualitative agreement with the theoretical speculations on the driving energy that is available for crack extension after initiation, in particular, that larger energies are stored at mode-II stress fields than at mode-I stress fields.

In summary, the investigations have shown: for the case of mode-II loaded cracks about one quarter of the energy stored of the tip of the original mother crack is used for building up the energy of the compressive notch tip stress field; thus, only the difference energy is available for subsequent crack propagating. Despite of this fact, much more energy remains for the failure event than for an equivalent mode-I case. Of course, an idealistic situation has been considered: The effect would become even larger for $K_{IIc} > K_{Ic}$, but smaller for $K_{IIc} < K_{Ic}$.

FAILURE MODE TRANSITION AT INCREASING LOADING RATES

Mode-I cracks when loaded dynamically show an instability and failure behaviour which is essentially the same as if the load would have been applied quasi-statically – with the only difference that certain characteristic values become changed [10, 11]. When mode-II cracks are loaded dynamically, e.g. by an impact event, however, the failure behaviour changes completely with respect to the quasi-static one; a failure mode transition is observed when the loading rate exceeds a certain limit value.

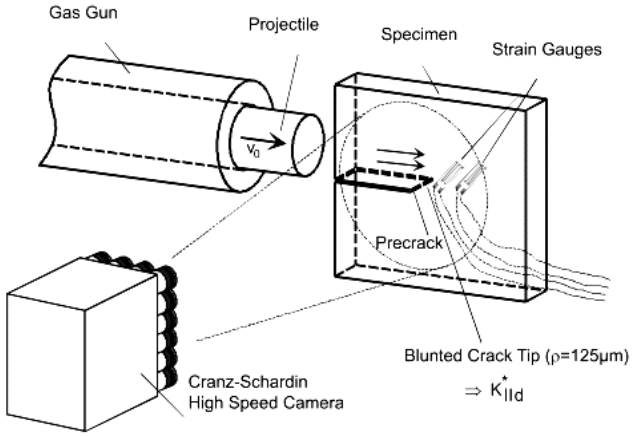

Fig. 10. Experimental set-up of the technique of loading edge cracks by edge impact and instrumentation, schematically.

The LECEI-technique (Loading of Edge Cracks by Edge Impact) [12-14], is used for generating high rate mode-II crack tip loading conditions. The principle of the loading tech-

nique is shown in Fig. 10. An edge cracked specimen is asymmetrically impacted at the cracked edge by a projectile accelerated by an air gun to velocities up to 100 m/s. The impinging projectile initiates a compressive wave to one side (above) the crack. To the other side of the crack (below) the specimen remains stress free. The displacements associated with the stress wave field generate a mode-II loading at the crack tip. The mode-II crack tip loading develops for the early time range of the impact event only, i.e. before waves that are reflected at the finite boundaries of the specimen will interfere with the crack tip again; this is the range of interest for high rate failure investigations. Since the boundary of the specimen is not of any influence for the time range of interest, it is not necessary to hold the specimen in a special loading fixture; the specimen is completely free.

Shadow optical investigations [13] have shown that the LECEI-technique yields an almost undisturbed mode-II loading for times before elastic waves reflected at the finite boundaries of the specimen interfere with the crack tip again. Some influence of a superimposed mode-I loading results for the very beginning of the impact event, which is due to lateral deformations associated with the compressive stress wave generated by the impact event; for later times, however, the mode-II loading is dominating and the superimposed mode-I loading becomes negligible.

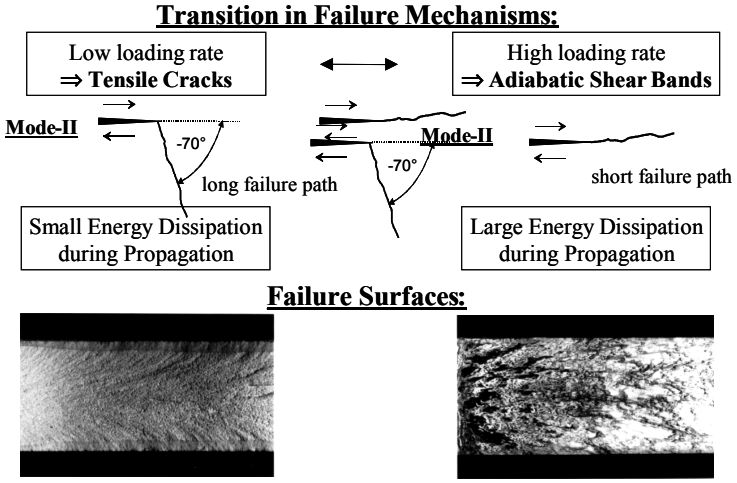

Fig. 11. Failure mode transition from tensile cracks to adiabatic shear bands at increasing levels of loading rate.

The failure behaviour at increasing levels of loading rate has been investigated by tests with impact velocities ranging from 10 to 100 m/s. Specimens made of the steel X2 NiCoMo 18 9 5 where tested. The typical specimen dimensions were about 100 × 200 mm; a projectile was utilized made of the same steel as the specimen, measuring 50 mm in diameter. The following results were obtained (see Fig. 11): At low loading rates, a failure behaviour is observed similar as in the quasi-static case: The mode-II loaded crack fails by a tensile mode-I crack propagating at an angle of about -70° with respects to the ligament; the generated failure surface shows the usual characteristics of a fracture surface, i.e. roughness as it is typical for the steel investigated and shear lips at the edges of the specimen. At high loading rates, the mode-II loaded crack fails by another mechanism, by an adiabatic shear band

propagating almost in the direction of the ligament (more precisely, the band propagates at an angle of a few degrees in the positive direction, i.e. to the opposite side of the ligament the mode-I crack would propagate). The failure surface has a smeared over, mirror-like, shiny appearance; shear lips at the edges of the specimen cannot be identified at all. In the high rate experiments, carried out with high impact velocities by which large amounts of energy are transferred to the specimen, the generated adiabatic shear bands come to arrest after a short propagation length only. In low rate experiments, carried out with low impact velocities by which smaller amounts of energy are transferred to the specimen, the generated cracks propagate entirely through the specimen separating the specimen into two halves and, thus, result in considerably larger propagation lengths. It is speculated, therefore, that adiabatic shear bands absorb more energy for propagation than cracks [13, 14]. Tests with initial cracks/notches of different bluntness have shown that the limit velocity for failure mode transition is the higher the more blunted the initial crack or notch.

The failure mechanism of adiabatic shear bands is less well understood than the usual fracture process: Due to the quasi-adiabatic conditions that control the high rate failure process of adiabatic shear bands, the generation of plastic deformations at the tip of the initial crack results in high temperature values leading to a thermal softening and shear localization in turn, processes which represent the basis for the formation of adiabatic shear bands. The adiabatic shear bands either show a deformed structure (deformed bands) or phase transformations to a martensitic structure take place, which are made visible by a white edging band (transformed bands); examples are given in Fig. 12. The hardness and the strength of the material inside the adiabatic shear band are considerably higher than of the base material, in particular this is the case for transformed bands. The final failure of adiabatic shear bands can be caused by fracture or by void growth and coalescens processes, mechanisms which require small amounts of energy compared to the energy necessary for the formation of the adiabatic shear band itself. For further information on adiabatic shear bands in general see e.g. [15].

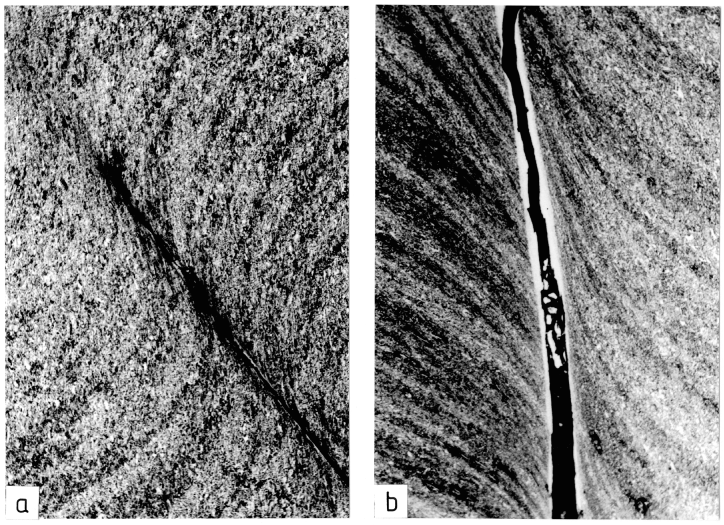

Fig. 12. Micrographs of adiabatic shear bands; (a) deformed band, steel: X2 NiCoMo 18 9 5, (b) transformed band, steel: 42 CrMo 4.

INFLUENCE OF LOADING RATE ON SHEAR FRACTURE TOUGHNESS FOR FAILURE MODE TRANSITION

The dependence of the impact shear mode-II fracture toughness, denoted K_{IId}, has been investigated by Bürgel and Kalthoff [16, 17] as a function of loading rate, in particular in the regime of failure mode transition from cracks to adiabatic shear bands; i.e. in the regime where the failure mode changes from a low to a high energy dissipation process.

High rate shear mode-II experiments are performed using the LECEI-technique as described in the previous chapter. For determining mode-II intensity factors during the phase of loading, a strain gauge measuring technique has been developed following the ideas introduced by Dally, Sandford [18] for the mode-I case. The principle of this technique was adopted and modified to apply for mode-II loading situations [16, 19]. The specimen in the region near the crack tip is instrumented by a strain gauge. With respect to the crack tip the strain gauge location is characterized by the polar coordinates r and φ, the measuring direction is given by the angle α, Fig. 13.

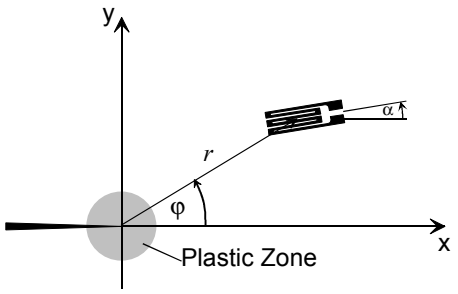

Fig. 13. Strain Gauge Location

The principle for determining stress intensity factors from the intensity of $1/\sqrt{r}$-crack tip stress singularity, on the one hand, requires small application distances r for achieving high accuracy results. Due to plasticity effects, i.e. the formation of a plastic zone around the crack tip, however, the minimum application distance r is limited; it has to be sufficiently large with respect to the size of the crack tip plastic zone to ensure that the stress field is dominated by the $1/\sqrt{r}$-dependence. For large distances from the crack tip, on the other hand, the influence of higher order terms of the crack tip stress field increases and, consequently, their disturbing influence has to be considered. The two free application parameters, the angles φ and α, can now be chosen in such a way that the two higher order terms are eliminated or minimized. For $\nu = 0.3$ the optimum application angles are

$$\varphi_{opt} \approx 10°, \qquad \alpha_{opt} \approx 60°. \tag{4}$$

Because of the still remaining and principally unavoidable influence of next higher order terms, two strain gauges are used (as shown in Fig. 10) in order to allow for an extrapolation of the data towards the actual crack tip position. Furthermore, the strain gauges are calibrated in a quasi-static pre-experiment at a low load level, which does not influence the loading situation of the later main experiment. Verification studies [16] showed good agreement.

The time at which instability occurs, i.e. instability due to failure by a crack or by an adiabatic shear band, is deduced from the strain gauge records as well. When failure occurs by a tensile crack propagating at an angle of about -70° with respect to the ligament, the distance between the advancing crack tip and the strain gauge becomes larger (see Fig. 10) and the strain gauge signal in turn will decrease. On the other hand, when failure occurs by an adiabatic shear band propagating almost in the direction of the ligament - more precisely at an angle of a few degrees in the positive direction with respect to the ligament - the adiabatic shear band propagates directly towards the strain gauge (see Fig. 10), i.e. the distance between the tip of the advancing shear band and the strain gauge becomes smaller and the strain gauge signal in turn will increase. These characteristics of the strain gauge record for times at and after instability represent clear indications not only of the time of onset of failure but also on the type of failure (in addition to direct observations).

Impact shear fracture toughnesses at increasing levels of loading rate have been determined with a 1 % chromium steel, German designation 42 CrMo 4. The steel was heat treated at 860 °C (2 h), quenched (oil) and tempered at 160 °C (3 h). In its final condition the steel showed a yield strength σ_{YS} of 1570 MPa and a tensile mode-I fracture toughness, K_{Ic}, of about 100 MN/m$^{3/2}$ (for an initial crack of ρ = 125 µm bluntness). The specimen size was 150 mm × 150 mm, the thickness of the specimens was 20 mm, the specimens were prepared with initial cracks/notches of about 60 mm length oriented in TL-direction. The tip of the initial notch/crack was blunted to a finite radius of 125 µm, the determined fracture toughnesses, thus, are not true fracture toughness values that apply for a sharp precrack, but toughnesses for a crack of finite bluntness are measured and, consequently, are characterized by the symbol K^{*}_{IId}.

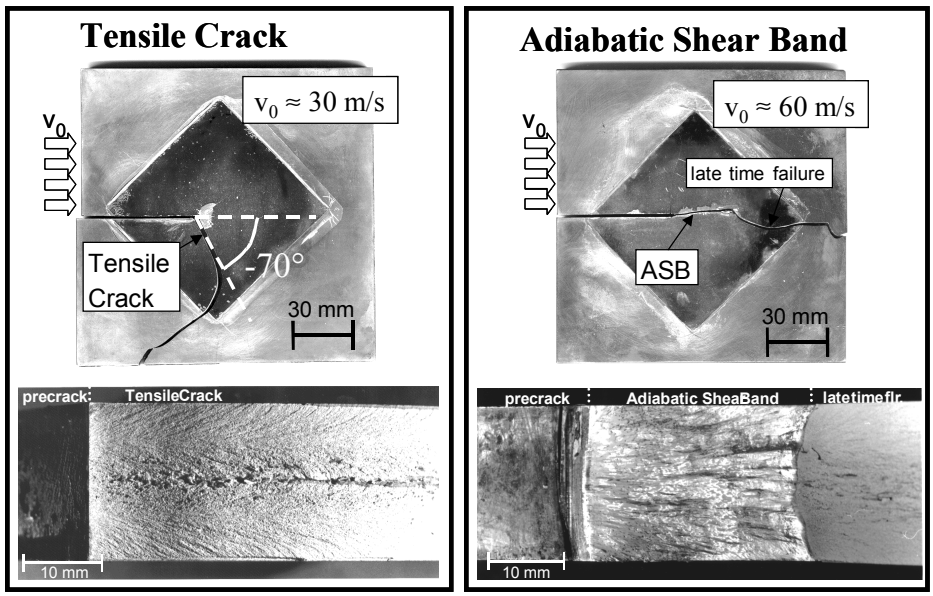

Fig. 14. Failure in steel 42 CrMo 4 by tensile cracks or adiabatic shear bands in the low or high rate regime.

Typical results from the series of experiments with impact velocity ranging from 20 m/s to 90 m/s are given in Fig. 14. Failure paths and failure surfaces are shown on the left hand side of the figure for a low rate experiment (30 m/s impact velocity) and on the right hand side of the figure for a high rate experiment (60 m/s impact velocity). In the low rate experiment, failure occurs by a tensile crack propagating at an angle of about –70° with respect to the ligament (for the beginning of the failure path); the failure surface is a typical fracture surface with roughness (plus additional indications of delamination in the middle of the specimen) and shear lips at the edges of the specimen, although small in size because of the high yield strength of the material. In the high rate experiment, failure due to an adiabatic shear band is observed propagating almost straight in the direction of the ligament (more precisely in the direction of few degrees to the opposite side of the ligament tensile cracks would propagate). The adiabatic shear band propagates over a considerable length (about 30 mm) and then is arrested. The length of the shear band at the edges of the specimen in all cases is larger than in the middle of the specimen, a behaviour opposite to the one observed for cracks. The failure following the adiabatic shear band is due to late time effects, e.g. due to arbitrary impact events in the catcher tank, when the specimen is decelerated. The adiabatic shear band has the typical shiny, mirror-like appearance; shear lips cannot be identified.

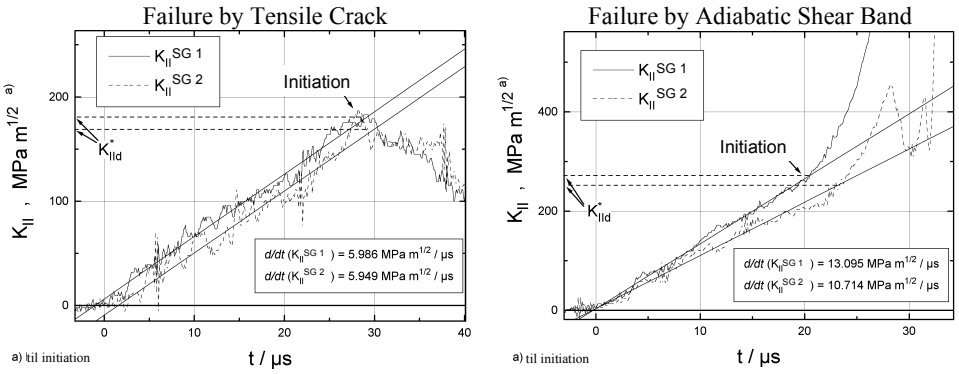

Fig. 15. Strain gauge response for failure by tensile cracks and adiabatic shear bands in steel 42 CrMo 4.

Figure 15 gives typical strain gauge signals with the strains converted to stress intensity factors obtained in a low and a high rate test. The signals of both strain gauges SG1 and SG2 are shown. During the loading phase, a more or less constant rise of the stress intensity factor K_{II} results with time t. In the low rate experiment, an abrupt change of the signal to a decreasing slope is observed, indicating failure by a tensile crack. In the high rate experiment, on the other hand, the slope of the strain gauge signal from a certain time on gets steeper, indicating failure by an adiabatic shear band. The times for these characteristic changes of the slope represent the times of instability, i.e. of onset of failure; the corresponding stress intensity factors represent the fracture toughness values K^{*}_{IId}.

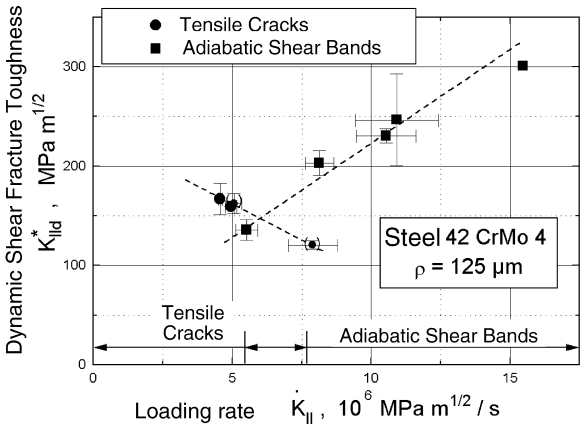

Fig. 16. Dependence of shear fracture toughness from loading rate for failure mode transition in steel 42 CrMo 4.

The shear mode-II fracture toughnesses measured as function of loading rate are shown in Fig. 16. Depending on which failure mode gets activated a different rate dependence is observed. For failure by tensile cracks which is obtained in low rate tests for loading rates $\dot{K}_{II} < 7 \cdot 10^6$ MNm$^{-3/2}$s^{-1}, the shear mode-II fracture toughness K^*_{IId} decreases with loading rate, a behaviour as it is regularly observed for mode-I loading as well. But, for failure by adiabatic shear bands, which results in the high rate tests for loading rates $\dot{K}_{II} > 7 \cdot 10^6$ MNm$^{-3/2}$s^{-1}, the shear mode-II fracture toughness K^*_{IId} shows an increasing trend with loading rate. The change between the two failure modes is not abrupt, a transition regime is observed for which the one or the other failure mode can become activated. There is no jump of the shear mode-II fracture toughness in this transition regime, the two curves overlap with their individual tendencies maintained. Data on specimens with different crack/notch tip bluntness show an equivalent behaviour [16].

The decreasing trend of the fracture toughness with loading rates for crack failure is certainly due to the regular strain rate hardening effects: with increasing loading rate the yield strength of the material increases, i.e. the resulting plastic zone at the crack tip and in turn the fracture toughness decreases. The increasing trend of the fracture toughness with loading rate for failure by adiabatic shear bands is speculated to be caused by thermal softening effects which are a result of the adiabatic conditions and extreme increases in temperature that control the process of adiabatic shear band failure: yielding of the material and plasticity effects become more pronounced which dissipate more energy, and thus, result in higher fracture toughness values with increasing loading rate. The processes in detail are more complicated in nature of course. Figure 17 shows micrographs of regions underneath the failure surfaces formed by a tensile crack and by an adiabatic shear band. In the case of failure by the tensile crack, the base material with its characteristic structure extends completely up to the failure surface. In the case of failure by the adiabatic shear band, the extreme heating effects result in phase transformations of the shear band zone adjacent to the failure surface which are accompanied by an increase of the hardness of the material.

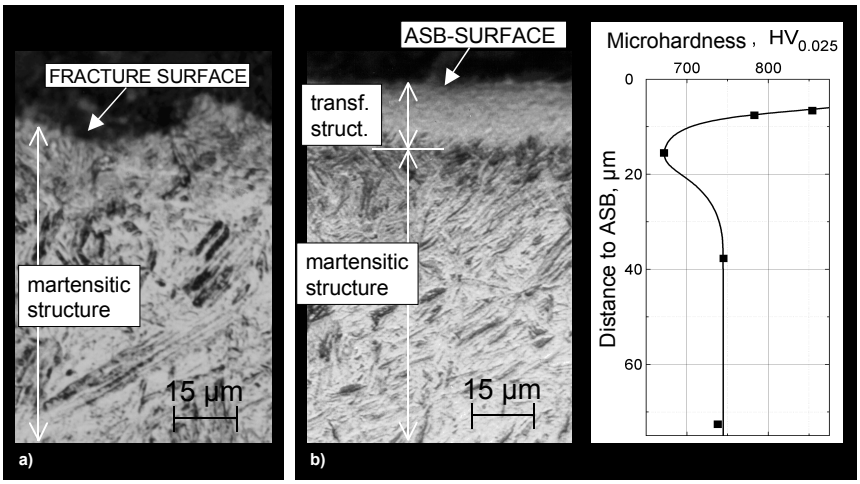

Fig. 17. Transformation of the microstructure and increase in micro-hardness in the vicinity of an adiabatic shear band (b) compared to the behaviour near a fracture surface (a).

SUMMARY AND CONCLUSIONS

The presented results show that the failure behaviour of mode-II loaded cracks is very different and far more complicated than the failure behaviour of mode-I loaded cracks:

1) Mode-II crack tip plastic zones are considerably larger than equivalent mode-I crack tip plastic zones, and, therefore, the in-plane dimensions of mode-II test pieces have to be considerably larger than for mode-I cases to fulfill the conditions of linear-elastic or small scale yielding conditions.
2) The instability process of mode-II loaded cracks is very different from the one of mode-I loaded cracks: in the mode-II case, a notch is formed between the initiated kinked crack and the original mother crack at which a compressive stress concentration builds up. The energy for building up this stress concentration field is taken from the energy field around the mode-II loaded mother crack and, thus, is not available for propagation of the initiated kinked crack. Despite of this effect, the strain energy release rate of a mode-II initiated crack is considerably higher than of an equivalent mode-I initiated crack, since the energy density of a mode-II crack tip stress field is much higher than of an equivalent mode-I crack tip field.
3) When mode-II loading of a crack is applied dynamically, a failure mode transition is observed when the loading rate exceeds a certain limit value: at low loading rates a kinked tensile mode-I crack is initiated propagating at an angle of about 70° with respect to the ligament, at high loading rates above a certain limit value failure by an adiabatic shear band is initiated, propagating practically in the direction of the ligament.
4) The shear mode-II fracture toughness K_{IId} decreases with loading rate when failure occurs by tensile cracks; but, it increases with loading rate when failure results by adiabatic shear bands.

The established findings show that a generalization of the mode-I case to a mode-II case is not possible on principle grounds, it can lead to erroneous results; only the mode-II case which is more general in nature can be reduced to the simpler mode-I case.

REFERENCES

1. Kalthoff, J.F., Failure Methodology of Mode-II Loaded Cracks, Int. J. on Complexity and Frontiers in Strength and Fracture, to be published
2. ASTM E399-90, Standard Test Method for Plane-Strain Fracture Toughness of Metallic Materials, American Society for Testing and Materials, Annual Book of ASTM Standards, Vol. 03.01, Philadelphia, pp. 412.
3. Hiese, W. and Kalthoff, J.F. (1998) Determination of Valid Mode-II Fracture Toughnesses K_{IIc}, Mixed-Mode Crack Behavior, ASTM STP 1359, (McDowell, D.L. and Miller, K.J., Editors), American Society for Testing and Materials, West Conshohocken, PA, pp. 74.
4. Hiese, W. (1999) Gültigkeitskriterien zur Bestimmung von Scherbruchzähigkeiten (Validity Criteria for Determining Shear Fracture Toughnesses), Dissertation, Ruhr-Universität Bochum, Germany.
5. Banks-Sills, L. and Arcan, M. (1983) An Edge-Cracked Mode II Fracture Specimen, Experimental Mechanics, vol.23, pp. 257.
6. Richard, H.A. (1981) Eine Bruchmechanikprobe zur Bestimmung von K_{IIc}-Werten (A Fracture Mechanics Specimen for Determining K_{IIc}-Values), Schweißen und Schneiden, vol.33, pp. 606.
7. Podleschny, R. (1995) Untersuchungen zum Instabilitätsverhalten scherbeanspruchter Risse (On the Instability Behavior of Shear Loaded Cracks), Dissertation, Ruhr-Universität Bochum, Germany.
8. Podleschny, R. and Kalthoff, J.F. (1994) A Novel Mode-II Fracture Criterion, Proc. 10th European Conference on Fracture, Structural Integrity: Experiments, Models and Applications, (Berger, C. and Schwalbe, K.-H., Editors), Engineering Materials Advisory Services Ltd., West Midlands, UK, pp. 211.
9. Kalthoff, J.F. (1993) Shadow Optical Method of Caustics, Chapter 9, In Handbook on Experimental Mechanics, (Kobayashi, A.S., Editor), Second Revised Edition, VCH Publishers, New York, pp. 407.
10. Klepaczko, J.R. (1982) Discussion of a New Experimental Method in Measuring Fracture Initiation Toughness at High Loading Rates by Stress Waves, J. Engng. Mat. and Tech., Trans ASME, vol.104, pp. 29.
11. Kalthoff, J.F. (1986) Fracture Behavior Under High Rate Loading, Engineering Fracture Mechanics, vol.23 Special Issue on Dynamic Fracture Mechanics, pp. 289.
12. Kalthoff, J.F. and Winkler, S. (1988) Failure Mode Transition at High Rates of Shear Loading, Proceedings of the International Conference on Impact Loading and Dynamic Behavior of Materials (Chiem, C.Y., Kunze, H.-D. and Meyer L.W., Editors), Deutsche Gesellschaft für Metallkunde, DGM-Verlag, Oberursel, pp. 185.
13. Kalthoff, J.F. (1990) Transition in the Failure Behaviour of Dynamically Shear Loaded Cracks, Proceedings of the 11th U.S. National Congress of Applied Mechanics (Chen, D.F., Editor), Tuscon, Arizona, May 21-25 1990, also Applied Mechanics Review, vol.43, pp. 247.
14. Kalthoff, J.F. (2000) Modes of Dynamic Shear Failure in Solids, International Journal of Fracture, vol.101, pp. 1.
15. Bai, Y. and Dodd, B. (1992) Adiabatic Shear Localization - Occurrence, Theories and Applications, Pergamon Press, Oxford
16. Bürgel A. (2000) Bruchmechanische Kennwerte beim Wechsel im Versagensverhalten dynamisch scherbeanspruchter Risse (Fracture Mechanics Properties for Failure Mode Transition of Dynamically Shear Loaded Cracks), Dissertation, Ruhr-Universität Bochum, Germany.
17. Kalthoff, J.F. and Bürgel, A. (2001) Influence of Loading Rate on Shear Fracture Toughness for Failure Mode Transition, Proceedings of the 10th Conference on Fracture, (Ravi-Chandar, Editor), Elsevier Science, Oxford, UK, 1096.
18. Dally, J.W. and Sanford, R.J. (1987) Strain-Gage Methods for Measuring the Opening-Mode Stress Intensity Factor K_I , Exp. Mech., vol.27, pp. 381.
19. Bürgel, A., Shin, H.S., Bergmannshoff, D. and Kalthoff, J.F. (1999) Optimization of the Strain-Gauge-Method for Measuring Mode-II Stress Intensity Factors, Proc. VII. Bilateral Czech/German Symposium: Significance of Hybrid Method for Assessment of Reliability and Durability in Engineering Sciences, 13.-15. April 1999 Liblice, Czech Republic, pp. 11.

METODIKA LOMA OPTEREĆENIH PRSLINA MODA II

Jörg F. Kalthoff

Razmatraju se različiti aspekti ponašanja pri lomu koji započinju iz opterećenih prslina moda II: kriterijumi validnosti i minimalni prohtevi veličine uzorka za merenje žilavosti loma K_{IIc}; ravnoteža energije procesa inicijacije uvojitih prslina uključujući kompresivne koncentracije napona vrhova ureza; prelaz moda loma sa tegljivih prslina na adijabatske smicajne trake pri visokim stopama opterećenja; zavisnost stope opterećenja dinamične žilavosti loma K_{IId} u režimu prelaza moda loma. Prikazani su nalazi studija na ove teme, i razmotrene implikacije rezultata za praktične primene. Utvrdjeno je da je ponašanje pri lomu opterećenih prslina moda II veoma drugačije i daleko složenije od opterećenih prslina moda I, tako da uopštavanja sa moda I na mod II mogu dovesti do jako velikih grešaka.